Electrical Power and Energy Systems 155 (2024) 109522

Contents lists available at ScienceDirect

International Journal of Electrical Power and Energy Systems

journal homepage: www.elsevier.com/locate/ijepes

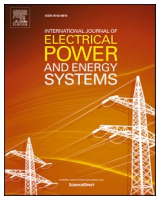

An accurate unsynchronized fault location method on practically transposed transmission lines with closed-form solutions

Dian Lu [a,b,c], Yu Liu [a,*], Yuhao Xie [a], Yuxuan Zhu [a], Rui Fan [d]

[a] School of Information Science and Technology, ShanghaiTech University, 393 Middle Huaxia Rd, Shanghai 201210, China
[b] Shanghai Advanced Research Institute, Chinese Academy of Sciences, Shanghai, China
[c] University of the Chinese Academy of Sciences, Beijing, China
[d] Department of Electrical & Computer Engineering, University of Denver, Denver, CO 80208, United States

ARTICLE INFO

Keywords:
Fault location
Unsynchronized measurements
Practically transposed lines
Fully distributed parameter model
Closed-form solution

ABSTRACT

This paper proposes an unsynchronized two-terminal fault location method on three phase practically transposed transmission lines.

Compared to the existing fault location methods, the proposed method considers the asymmetry of the practically transposed transmission lines during the fault in practice. First, the proposed method constructs the practically transposed transmission lines by connecting three untransposed transmission line sections. For each section, the fully distributed parameters line model is adopted to ensure the modeling accuracy. According to the physical laws that the line should obey, the unsynchronized angle is estimated with analytical formulation before the fault. Next, the closed-form solutions of fault location are derived for different fault events, to avoid the risks of unconvergence using the iterative algorithms. In the numerical experiments, the proposed method shows higher accuracy of fault location than the existing fault location methods, regardless of fault types, locations and impedances. The proposed method also demonstrates robustness against various unsynchronized angles, loading conditions, measurement noises and line lengths.

1. Introduction

With the global goal of carbon neutrality, renewable power generations such as wind power generation and photovoltaic power generation have been vigorously developed. Transmission lines are essential components of power systems to connect renewable resources to consumers, to ensure availability of low carbon and clean energy. During power system operation, transmission lines may fail sometimes due to the occurrence of internal line faults. In order to clear the fault, accurate fault location techniques speed up the process of finding the fault and shorten the time needed for restoration, so as to improve the power supply reliability. Researchers proposed abundant fault location methods in the existing literatures [1–5]. Existing fault location methods can be mainly classified into the traveling-wave based methods, data driven methods, time domain based methods and the fundamental frequency phasor based methods. The traveling-wave based methods detect the arrival time of wavefronts at line terminals to locate the fault. When the high fault impedance cases occur or the inception angle of the fault is close to zero, the traveling-wave based methods may face wavefront detection challenges. Also, high accuracy of fault location usually requires high sampling rates, leading to additional costs [6–7]. Data driven methods usually require big dataset with high quality training data, which may be not adequate for practical power systems [8–9]. Time domain based methods locate the fault by combining the transient measurements with line model to solve the location of the fault. Nevertheless, building accurate line model could be challenging within transient process during the fault [10]. Compared to those methods, the fundamental frequency phasor based methods are the most widely adopted methods in practical AC power systems, as they can be implemented by simply utilizing the three phase voltage and current phasor measurements available from substations [11–12]. These methods locate the fault by solving the phasor domain equations, which are based on the physical laws that transmission lines should obey. Next, this paper focuses on the fundamental frequency phasors based methods.

The fundamental frequency phasor based methods mainly contain one terminal methods and two terminal methods. The one terminal methods utilize the three phase voltage and current phasors at local

* Corresponding author.
E-mail address: liuyu@shanghaitech.edu.cn (Y. Liu).

https://doi.org/10.1016/j.ijepes.2023.109522
Received 30 November 2022; Received in revised form 14 March 2023; Accepted 21 September 2023
Available online 30 September 2023

terminal to determine the location of the fault, and the fault location accuracy may be influenced by the source impedances and fault impedances [13]. To improve the accuracy of fault location, two-terminal based methods are proposed. These methods usually require the three phase voltage and current phasors at both terminals [14–15]. If satellite time references are available for measurements at both terminals, synchronized voltage and current phasors can be utilized directly to locate the fault [16–17]. There are also methods to locate faults with unsynchronized measurements [18–19]. For types of transmission lines, they include transposed lines and untransposed lines. The untransposed lines usually present slight unbalance among three phases due to the asymmetrical geometric structure of the tower. Therefore, the untransposed lines are usually short lines and most long transmission lines are transposed. The transposed lines exchange the position of conductors according to a certain principle [20].

For the transposed transmission lines, the existing fault location methods often adopt the sequence component method to locate the fault. Literature [21] proposes the fault location method by utilizing the positive sequence impedances of the lines with a noniterative solution, and the synchrophasors at both terminals are required. On the one hand, this method neglects the shunt admittance of the lines and it may lead to errors for fault location algorithm when the transmission lines are long or the fault occurs with high fault impedances. Literature [22] proposed the fault location method without requiring the synchronized measurements. Meanwhile, this method considers the distributed parameter line model to improve the accuracy of fault location. As this method applies the Newton's method to find the fault with the iterative procedure, the selection of initial values and the risks of converging to local optimum or even diverging may affect the accuracy of the fault location in practice. Literature [23] proposed the new fault location method with analytical solution of fault location. It still considers the distributed parameter line model and can find the fault with unsynchronized measurements.

In fact, aforementioned fault location method [21–23] all assume that the transposed lines are ideally transposed during the fault, i.e. the transposition occurs at every small line section, and the line is homogeneous with fully symmetrical equivalent tower structure. Nevertheless, according to the principle of transposition in [20], the position of three phase conductors *A*, *B* and *C* are rotated every one-third of the total length. Therefore, the practically transposed transmission lines are usually constructed by three sections untransposed lines in series, and is in fact a non-homogeneous transmission line. Before the fault, the practically transposed lines are approximately equivalent to the ideally transposed lines. However, once the fault occurs on the untransposed lines, the non-homogeneity of the practically transposed lines should be considered because the balance of three phase is broken by the fault. Literature [24] mentioned the practically transposed lines model, but still the positive sequence component model is used for fault location, and the asymmetry of untransposed line sections are not fully considered. Literature [25] considered the fault location method on non-homogeneous transmission lines. However, this method requires synchronized measurements at both terminals and utilizes an iterative algorithm (with the risks of unconvergence) to solve the problem of fault location.

This paper proposes a closed-form solution of fault location for practically transposed transmission lines. First, the proposed method builds the practically transposed lines with three non-homogeneous untransposed line sections in series, to consider the line asymmetry during the fault. Meanwhile, the fully distributed parameter line model is adopted for each line section to ensure the accuracy of the line model. In addition, the unsynchronized angle between the measurements at both terminals is estimated before the fault. Afterwards, the location of the fault is carefully derived with closed-form solutions. Numerical experiments validate that the proposed method owns higher accuracy of fault location than the existing method with different fault locations, fault impedances and fault types. Furthermore, the proposed method presents the robustness with different unsynchronized angles, loading conditions, measurement noises and line length. The contributions of this paper are summarized as follows,

- The proposed method builds the practically transposed transmission lines model exactly from the physical connection of the line; with three untransposed line section in series, the practical asymmetry of the transposed lines are accurately considered during the fault;
- The fully distributed parameter untransposed line model is adopted to ensure accuracy of line model; the method does not require synchronized measurements at both terminals;
- With the complex model of the practically transposed transmission line, the closed-form solution of fault location is still obtained to avoid the risks of unconvergence for the iterative algorithm;
- The proposed method presents higher accuracy of fault location than the existing method under different fault scenarios.

The remainder of this paper is organized as follows. Section 2 analyses the necessity of a new fault location method on practically transposed lines. Section 3 introduces the details of derivations of the proposed fault location method on practically transposed lines. Section 4 shows the numerical experiments to verify the performance of the proposed method in comparison to the existing methods. Section 5 further studies the impact of different factors on the performance of the proposed method. Section 6 concludes this paper.

2. Necessity of a new fault location method for practically transposed lines

In fact, the existing fault location methods utilizing the sequence network components usually assume that the transmission lines are ideally transposed. There are differences between the practically transposed transmission lines and the ideally transposed transmission lines. Literature [20] reviews the principle of transposition, which exchanges physically the position of phase conductors *A*, *B* and *C* and the conductors are rotated every one-third of the total line length in general.

Fig. 1 (a) shows the practically transposed transmission lines before the fault. $\widetilde{V}_{abc}^{S,P}$, $\widetilde{V}_{abc}^{R,P}$, $\widetilde{I}_{abc}^{S,P}$ and $\widetilde{I}_{abc}^{R,P}$ are the three phase voltage and current phasors of measurements at both terminals before the fault, respectively. The superscripts '*S*' and '*R*' denotes the terminal *S* and terminal *R*, respectively. The subscripts '*abc*' denotes the three phase *A*, *B* and *C*. To ensure the synchronization of measurements, $e^{j\delta}$ is defined as the synchronization operator: the measurements at terminal *R* is multiplied by the operator to compensate the unsynchronization. As the elements of the practically transposed transmission lines, *l* is the length of every untransposed line section. From the terminal *S* and terminal *R* to view the total transmission lines, the practically transposed transmission lines can be treated as an ideally transposed transmission line approximately before the fault. However, the practically transposed transmission lines are different from the ideally transposed transmission lines during the fault.

Fig. 1 (b) shows the practically transposed lines when a fault occurs within the Section 1 untransposed line section as an example. $\widetilde{V}_{abc}^{S,F}$, $\widetilde{V}_{abc}^{R,F}$, $\widetilde{I}_{abc}^{S,F}$ and $\widetilde{I}_{abc}^{R,F}$ are the three phase voltage and current phasors measurements at both terminals during the fault, respectively. $x{\cdot}l$ expresses the distance between the location of the fault and the terminal *S*. $\widetilde{I}_{abc}^{f1,F}$ and $\widetilde{I}_{abc}^{f2,F}$ are the three phase current phasors flowing into the fault position. $\widetilde{V}_{abc}^{f,F}$ are the three phase voltage phasors at the fault position. The line at the left side of the fault is an untransposed line with xl length. The line at the right side of the fault is a non-homogeneous transmission line with $(3\text{-}x)l$ length. Therefore, one can clearly observe that the ideally transposed assumptions will lead to errors of fault location during the fault, and it is necessary to propose a new fault location method to consider

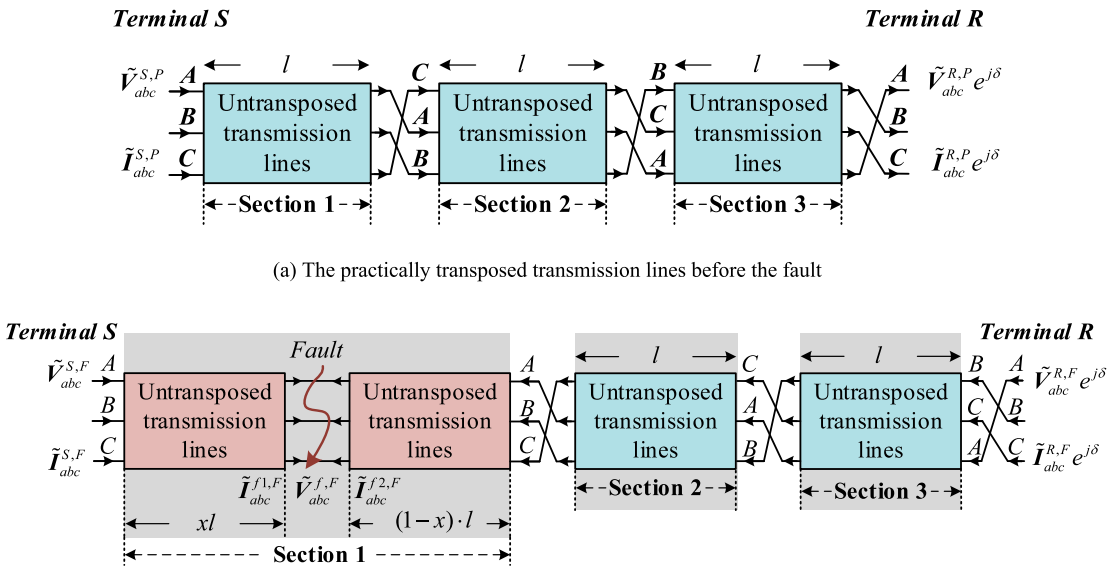

(a) The practically transposed transmission lines before the fault

(b) The practically transposed transmission lines during the fault

Fig. 1. The practically transposed transmission lines.

the asymmetry of the practically transposed lines.

On one hand, the new fault location method needs to guarantee the accuracy of fault location; in this case, the model of the practically transposed line is more complex than that of the ideally transposed line. On the other hand, the new fault location method should still try to come up with a closed-form noniterative solution. Also, even with the unsynchronized measurements at both terminals, the new fault location method should be applicable as well.

3. Proposed fault location method considering asymmetry of practically transposed lines

This section expresses the proposed fault location method on practically transposed transmission lines in detail. First, the proposed method considers the problems of unsynchronized measurements at both terminals and estimates the unsynchronized angle. After that, derivations of the proposed fault location method are shown with different fault events, and the closed-form noniterative solutions of fault location are obtained.

3.1. Estimation of the unsynchronized angle on practically transposed lines

In practice, the measurements at both terminals could be unsynchronized. Based on this motivation, the proposed fault location method considers the unsynchronized measurements at both terminals and calculate the synchronization operator $e^{j\delta}$ with closed-form noniterative solution.

In Fig. 1(a), the series impedance matrix and the shunt admittance matrix of the untransposed lines are as (1),

$$\mathrm{Z}_{abc}=\begin{bmatrix} Z_{aa} & Z_{ab} & Z_{ac} \\ Z_{ab} & Z_{bb} & Z_{bc} \\ Z_{ac} & Z_{bc} & Z_{cc} \end{bmatrix} \mathrm{Y}_{abc}=\begin{bmatrix} Y_{aa} & Y_{ab} & Y_{ac} \\ Y_{ab} & Y_{bb} & Y_{bc} \\ Y_{ac} & Y_{bc} & Y_{cc} \end{bmatrix} \tag{1}$$

To ensure the accuracy of line mode, the proposed method utilizes the fully distributed parameter line model. The authors' previous work [25] provides the physical laws that the untransposed lines should obey before the fault for considering the fully distributed parameter line model. Cascading the three line models in Fig. 1(a), the terminal voltages and currents have the following relationship,

$$\begin{bmatrix} \widetilde{\mathrm{V}}_{abc}^{R,P} \\ \widetilde{\mathrm{I}}_{abc}^{R,P} \end{bmatrix} e^{j\delta}=\mathrm{K}_1\mathrm{M}^{-1}e^{-l\mathrm{B}}\mathrm{M}\mathrm{K}_1\mathrm{M}^{-1}e^{-l\mathrm{B}}\mathrm{M}\mathrm{K}_1\mathrm{M}^{-1}e^{-l\mathrm{B}}\mathrm{M}\begin{bmatrix} \widetilde{\mathrm{V}}_{abc}^{S,P} \\ \widetilde{\mathrm{I}}_{abc}^{S,P} \end{bmatrix} \tag{2}$$

where matrix $\boldsymbol{K}_1$ is the transposition matrix to change the position of three phase conductors (eg. the three phase conductors exchange the order from *A*, *B*, *C* to *B*, *C*, *A* via the transposition). The definitions of matrix $\boldsymbol{K}_1$, matrix $\boldsymbol{M}$ and matrix $\boldsymbol{B}$ are defined as formula (3),

$$\mathrm{K}_1=\begin{bmatrix} 0 & 0 & 1 & 0 & 0 & 0 \\ 1 & 0 & 0 & 0 & 0 & 0 \\ 0 & 1 & 0 & 0 & 0 & 0 \\ 0 & 0 & 0 & 0 & 0 & 1 \\ 0 & 0 & 0 & 1 & 0 & 0 \\ 0 & 0 & 0 & 0 & 1 & 0 \end{bmatrix},\quad \mathrm{M}=\begin{bmatrix} \mathrm{I}_3 & 0 \\ 0 & \mathrm{Z}_{abc} \end{bmatrix},\quad \mathrm{B}=\begin{bmatrix} 0 & \mathrm{I}_3 \\ \mathrm{Z}_{abc}\mathrm{Y}_{abc} & 0 \end{bmatrix} \tag{3}$$

where 0 and I_3 are the zero matrix and identity matrix with the dimension of 3. One can observe that equation (2) includes 6 rows. Here the first row can be selected to calculate the synchronized operator $e^{j\delta}$. The first row of (2) can be rewritten as (4),

$$\widetilde{V}_a^{R,P}e^{j\delta}=J_{11}\widetilde{V}_a^{S,P}+J_{12}\widetilde{V}_b^{S,P}+J_{13}\widetilde{V}_c^{S,P}+J_{14}\widetilde{I}_a^{S,P}+J_{15}\widetilde{I}_b^{S,P}+J_{16}\widetilde{I}_c^{S,P} \tag{4}$$

J_{ij} (i and j denote the row and column indices of the matrix $(\mathrm{K}_1\mathrm{M}^{-1}e^{-l\mathrm{B}}\mathrm{M}\mathrm{K}_1\mathrm{M}^{-1}e^{-l\mathrm{B}}\mathrm{M}\mathrm{K}_1\mathrm{M}^{-1}e^{-l\mathrm{B}}\mathrm{M})$, respectively) are defined as (5),

$$\mathrm{K}_1\mathrm{M}^{-1}e^{-l\mathrm{B}}\mathrm{M}\mathrm{K}_1\mathrm{M}^{-1}e^{-l\mathrm{B}}\mathrm{M}\mathrm{K}_1\mathrm{M}^{-1}e^{-l\mathrm{B}}\mathrm{M}=\begin{bmatrix} J_{11} & J_{12} & J_{13} & J_{14} & J_{15} & J_{16} \\ J_{21} & J_{22} & J_{23} & J_{24} & J_{25} & J_{26} \\ J_{31} & J_{32} & J_{33} & J_{34} & J_{35} & J_{36} \\ J_{41} & J_{42} & J_{43} & J_{44} & J_{45} & J_{46} \\ J_{51} & J_{52} & J_{53} & J_{54} & J_{55} & J_{56} \\ J_{61} & J_{62} & J_{63} & J_{64} & J_{65} & J_{66} \end{bmatrix} \tag{5}$$

Because the three phase voltage and current phasors at both terminals and the line parameters are known, the synchronized operator $e^{j\delta}$ can be calculated as (6) according to (4),

$$e^{j\delta}=(J_{11}\widetilde{V}_a^{S,P}+J_{12}\widetilde{V}_b^{S,P}+J_{13}\widetilde{V}_c^{S,P}+J_{14}\widetilde{I}_a^{S,P}+J_{15}\widetilde{I}_b^{S,P}+J_{16}\widetilde{I}_c^{S,P})/\widetilde{V}_a^{R,P} \tag{6}$$

3.2. Fault location on practically transposed lines

As mentioned before, the practically transposed transmission line is a non-homogeneous line during the fault. Considering that fault may occurs within any untransposed line section, the proposed fault location method provides three different derivations of fault location, each corresponding to a fault within one untransposed line section.

(a) when the fault occurs on the section 1 line

Fig. 1 (b) shows the practically transposed lines when the fault occurs on Section 1. According to the physical laws during the fault, where $\boldsymbol{K}_2$ is also the transposition matrix and it is defined as (9),

$$\mathrm{M}^{-1}e^{-x\mathrm{l}\mathrm{B}}\mathrm{M}\begin{bmatrix}\widetilde{\mathrm{V}}_{abc}^{S,F} & \widetilde{\mathrm{I}}_{abc}^{S,F}\end{bmatrix}^{T}=\begin{bmatrix}\widetilde{\mathrm{V}}_{abc}^{f,F} & \widetilde{\mathrm{I}}_{abc}^{f1,F}\end{bmatrix}^{T} \tag{7}$$

$$\begin{aligned}&\mathrm{M}^{-1}e^{-(1-x)\mathrm{l}\mathrm{B}}\mathrm{M}\mathrm{K}_2\mathrm{M}^{-1}e^{-\mathrm{l}\mathrm{B}}\mathrm{M}\mathrm{K}_2\mathrm{M}^{-1}e^{-\mathrm{l}\mathrm{B}}\mathrm{M}\mathrm{K}_2\begin{bmatrix}\widetilde{\mathrm{V}}_{abc}^{R,F} & \widetilde{\mathrm{I}}_{abc}^{R,F}\end{bmatrix}^{T}e^{j\delta}\\&=\begin{bmatrix}\widetilde{\mathrm{V}}_{abc}^{f,F} & \widetilde{\mathrm{I}}_{abc}^{f2,F}\end{bmatrix}^{T}\end{aligned} \tag{8}$$

$$\mathrm{K}_2=\begin{bmatrix}0&1&0&0&0&0\\0&0&1&0&0&0\\1&0&0&0&0&0\\0&0&0&0&1&0\\0&0&0&0&0&1\\0&0&0&1&0&0\end{bmatrix} \tag{9}$$

Because the three phase measurement phasors at both terminals and the line parameters are known, and $e^{j\delta}$ has been solved by (6), the part $\mathrm{K}_2\mathrm{M}^{-1}e^{-\mathrm{l}\mathrm{B}}\mathrm{M}\mathrm{K}_2\mathrm{M}^{-1}e^{-\mathrm{l}\mathrm{B}}\mathrm{M}\mathrm{K}_2\begin{bmatrix}\widetilde{\mathrm{V}}_{abc}^{R,F} & \widetilde{\mathrm{I}}_{abc}^{R,F}\end{bmatrix}^{T}e^{j\delta}$ in equation (8) can be calculated and expressed with the formula (10),

$$\begin{bmatrix}\mathrm{N}_{11} & \mathrm{N}_{12}\end{bmatrix}^{T}=\mathrm{K}_2\mathrm{M}^{-1}e^{-\mathrm{l}\mathrm{B}}\mathrm{M}\mathrm{K}_2\mathrm{M}^{-1}e^{-\mathrm{l}\mathrm{B}}\mathrm{M}\mathrm{K}_2\begin{bmatrix}\widetilde{\mathrm{V}}_{abc}^{R,F} & \widetilde{\mathrm{I}}_{abc}^{R,F}\end{bmatrix}^{T}e^{j\delta} \tag{10}$$

where N_{11} and N_{12} are column vectors with the dimension 3, and all the values can be calculated by the formula $\mathrm{K}_2\mathrm{M}^{-1}e^{-\mathrm{l}\mathrm{B}}\mathrm{M}\mathrm{K}_2\mathrm{M}^{-1}e^{-\mathrm{l}\mathrm{B}}\mathrm{M}\mathrm{K}_2\begin{bmatrix}\widetilde{\mathrm{V}}_{abc}^{R,F} & \widetilde{\mathrm{I}}_{abc}^{R,F}\end{bmatrix}^{T}e^{j\delta}$. Note that throughout the paper the following convention holds, i.e. $\begin{bmatrix}(\cdot)_1 & (\cdot)_2\end{bmatrix}^{T}=\begin{bmatrix}(\cdot)_1\\(\cdot)_2\end{bmatrix}$. Substituting (10) into (8),

$$\mathrm{M}^{-1}e^{-(1-x)\mathrm{l}\mathrm{B}}\mathrm{M}\begin{bmatrix}\mathrm{N}_{11} & \mathrm{N}_{12}\end{bmatrix}^{T}=\begin{bmatrix}\widetilde{\mathrm{V}}_{abc}^{f,F} & \widetilde{\mathrm{I}}_{abc}^{f2,F}\end{bmatrix}^{T} \tag{11}$$

For equation (7), the decoupling procedure is rewritten as follows. The key idea is to convert the electric quantities from *abc* domain into another domain, i.e.,$\widetilde{\mathrm{V}}_{120}=\mathrm{T}_V^{-1}\widetilde{\mathrm{V}}_{abc}$ and $\widetilde{\mathrm{I}}_{120}=\mathrm{T}_I^{-1}\widetilde{\mathrm{I}}_{abc}$. Here $\widetilde{\mathrm{V}}_{abc}$ and $\widetilde{\mathrm{I}}_{abc}$ are general voltage and current vectors in abc domain, and $\widetilde{\mathrm{V}}_{120}$ and $\widetilde{\mathrm{I}}_{120}$ are corresponding voltage and current vectors in the new domain. It is worth noting that, although here the expression of "120" is utilized, they are just the notation of the new domain and not corresponding to positive/negative/zero sequences.

Because the line parameters $\boldsymbol{Z}_{\mathrm{abc}}$ and $\boldsymbol{Y}_{\mathrm{abc}}$ are known variables, the eigenvalue decomposition can be adopted to find the matrix $\boldsymbol{T}_{\mathrm{V}}^{1}$ as (12).

$$\mathrm{T}_V^{-1}\mathrm{Z}_{abc}\mathrm{Y}_{abc}\mathrm{T}_V=diag(\begin{bmatrix}\gamma_1^2 & \gamma_2^2 & \gamma_0^2\end{bmatrix}^{T}) \tag{12}$$

where diag(·) denotes the diagonal matrix with the elements γ_1^2, γ_2^2 and γ_0^2. Set $\mathrm{T}_I=\mathrm{T}_V^{-T}$, the formula (13) holds,

$$\mathrm{T}_I^{-1}\mathrm{Y}_{abc}\mathrm{Z}_{abc}\mathrm{T}_I=diag(\begin{bmatrix}\gamma_1^2 & \gamma_2^2 & \gamma_0^2\end{bmatrix}^{T}) \tag{13}$$

Then the new diagonal matrix can be obtained as (14),

$$\mathrm{T}_V^{-1}\mathrm{Z}_{abc}\mathrm{T}_I=diag(\begin{bmatrix}Z_1 & Z_2 & Z_0\end{bmatrix}^{T}) \tag{14}$$

For the matrix $\boldsymbol{B}$ in (3), it can be expressed as (15) via eigenvalue decomposition,

$$\mathrm{B}=\begin{bmatrix}0 & \mathrm{I}_3\\ \mathrm{Z}_{abc}\mathrm{Y}_{abc} & 0\end{bmatrix}=\mathrm{T}_S\begin{bmatrix}0 & \mathrm{I}_3\\ diag(\begin{bmatrix}\gamma_1^2 & \gamma_2^2 & \gamma_0^2\end{bmatrix}) & 0\end{bmatrix}\mathrm{T}_S^{-1} \tag{15}$$

where the matrix $\mathrm{T}_S=\begin{bmatrix}\mathrm{T}_V & 0\\ 0 & \mathrm{T}_V\end{bmatrix}$.

Similarly, the following term can also be expressed by diagonal matrices via eigenvalue decomposition,

$$\begin{bmatrix}0 & \mathrm{I}_3\\ diag(\begin{bmatrix}\gamma_1^2 & \gamma_2^2 & \gamma_0^2\end{bmatrix}) & 0\end{bmatrix}=\mathrm{T}_W\Lambda\mathrm{T}_W^{-1} \tag{16}$$

where

$$\begin{aligned}\mathrm{T}_W&=\begin{bmatrix}1&1&0&0&0&0\\0&0&1&1&0&0\\0&0&0&0&1&1\\\gamma_1&-\gamma_1&&&&\\&&\gamma_2&-\gamma_2&&\\&&&&\gamma_3&-\gamma_3\end{bmatrix},\quad\Lambda\\&=diag(\begin{bmatrix}\gamma_1 & -\gamma_1 & \gamma_2 & -\gamma_2 & \gamma_3 & -\gamma_3\end{bmatrix}^{T})\end{aligned} \tag{17}$$

According to (15) and (16), equation (18) can be obtained,

$$\begin{aligned}e^{-x\mathrm{l}\mathrm{B}}&=\sum_{m=0}^{\infty}\frac{(-x\mathrm{l}\mathrm{B})^m}{m!}=\sum_{m=0}^{\infty}\frac{(-x\mathrm{l}\mathrm{T}_S\mathrm{T}_W\Lambda\mathrm{T}_W^{-1}\mathrm{T}_S^{-1})^m}{m!}\\&=\mathrm{T}_S\mathrm{T}_W\left[\sum_{m=0}^{\infty}\frac{(-x\mathrm{l}\Lambda)^m}{m!}\right]\mathrm{T}_W^{-1}\mathrm{T}_S^{-1}\\&=\mathrm{T}_S\mathrm{T}_W diag(\begin{bmatrix}e^{-x\mathrm{l}\gamma_1} & e^{x\mathrm{l}\gamma_1} & e^{-x\mathrm{l}\gamma_2} & e^{x\mathrm{l}\gamma_2} & e^{-x\mathrm{l}\gamma_0} & e^{x\mathrm{l}\gamma_0}\end{bmatrix}^{T})\mathrm{T}_W^{-1}\mathrm{T}_S^{-1}\\&=\mathrm{T}_S\begin{bmatrix}\mathrm{S}_{11} & \mathrm{S}_{12}\\ \mathrm{S}_{21} & \mathrm{S}_{22}\end{bmatrix}\mathrm{T}_S^{-1}\end{aligned} \tag{18}$$

where

$$\begin{aligned}\mathrm{S}_{11}=\mathrm{S}_{22}&=diag(\begin{bmatrix}\cosh(-x\mathrm{l}\gamma_1) & \cosh(-x\mathrm{l}\gamma_2) & \cosh(-x\mathrm{l}\gamma_0)\end{bmatrix}^{T})\\\mathrm{S}_{12}&=diag(\begin{bmatrix}\frac{\sinh(-x\mathrm{l}\gamma_1)}{\gamma_1} & \frac{\sinh(-x\mathrm{l}\gamma_2)}{\gamma_2} & \frac{\sinh(-x\mathrm{l}\gamma_0)}{\gamma_0}\end{bmatrix}^{T})\\\mathrm{S}_{21}&=diag(\begin{bmatrix}\gamma_1\sinh(-x\mathrm{l}\gamma_1) & \gamma_2\sinh(-x\mathrm{l}\gamma_2) & \gamma_0\sinh(-x\mathrm{l}\gamma_0)\end{bmatrix}^{T})\end{aligned} \tag{19}$$

Then, equation (7) can be converted to the new domain, as (20),

$$\begin{aligned}\begin{bmatrix}\widetilde{\mathrm{V}}_{120}^{f,F}\\ \widetilde{\mathrm{I}}_{120}^{f1,F}\end{bmatrix}&=\begin{bmatrix}\mathrm{T}_V & 0\\ 0 & \mathrm{T}_I\end{bmatrix}^{-1}\mathrm{M}^{-1}e^{-x\mathrm{l}\mathrm{B}}\mathrm{M}\begin{bmatrix}\mathrm{T}_V & 0\\ 0 & \mathrm{T}_I\end{bmatrix}\begin{bmatrix}\widetilde{\mathrm{V}}_{120}^{S,F}\\ \widetilde{\mathrm{I}}_{120}^{S,F}\end{bmatrix}\\&=\begin{bmatrix}\mathrm{S}_{11} & \mathrm{R}_{12}\\ \mathrm{R}_{21} & \mathrm{S}_{22}\end{bmatrix}\begin{bmatrix}\widetilde{\mathrm{V}}_{120}^{S,F}\\ \widetilde{\mathrm{I}}_{120}^{S,F}\end{bmatrix}\end{aligned} \tag{20}$$

where

$$\begin{aligned}\mathrm{R}_{12}&=diag(\begin{bmatrix}Z_1\sinh(-x\mathrm{l}\gamma_1)/\gamma_1 & Z_2\sinh(-x\mathrm{l}\gamma_2)/\gamma_2 & Z_0\sinh(-x\mathrm{l}\gamma_0)/\gamma_0\end{bmatrix}^{T})\\\mathrm{R}_{21}&=diag(\begin{bmatrix}\gamma_1\sinh(-x\mathrm{l}\gamma_1)/Z_1 & \gamma_2\sinh(-x\mathrm{l}\gamma_2)/Z_2 & \gamma_0\sinh(-x\mathrm{l}\gamma_0)/Z_0\end{bmatrix}^{T})\end{aligned} \tag{21}$$

Therefore, $\widetilde{V}_1^{f,F}$ can be selected for calculating the location of the fault. From (20) and (21), $\widetilde{V}_1^{f,F}$ can be expressed as (22),

$$\widetilde{V}_1^{f,F}=\cosh(-\gamma_1 xl)\widetilde{V}_1^{S1,F}+Z_1\sinh(-\gamma_1 xl)\widetilde{I}_1^{S1,F}/\gamma_1 \tag{22}$$

where the superscripts "1" denotes the scenario where the fault occurs within section 1, and,

$$\begin{bmatrix} T_V & 0 \\ 0 & T_I \end{bmatrix}^{-1} \begin{bmatrix} \tilde{V}_{abc}^{S,F} \\ \tilde{I}_{abc}^{S,F} \end{bmatrix} = \begin{bmatrix} \tilde{V}_1^{S1,F} & \tilde{V}_2^{S1,F} & \tilde{V}_0^{S1,F} & \tilde{I}_1^{S1,F} & \tilde{I}_2^{S1,F} & \tilde{I}_0^{S1,F} \end{bmatrix}^T \quad (23)$$

Because equation (11) is similar as equation (7), the above procedure can be similarly applied,

$$\tilde{V}_1^{f,F} = \cosh[-\gamma_1(1-x)l]\tilde{V}_1^{R1,F} + Z_1 \sinh[-\gamma_1(1-x)l]\tilde{I}_1^{R1,F}/\gamma_1 \quad (24)$$

where the superscripts "1″ denotes the scenario where the fault occurs within section 1, and,

$$\begin{bmatrix} T_V & 0 \\ 0 & T_I \end{bmatrix}^{-1} \begin{bmatrix} N_{11} \\ N_{12} \end{bmatrix} = \begin{bmatrix} \tilde{V}_1^{R1,F} & \tilde{V}_2^{R1,F} & \tilde{V}_0^{R1,F} & \tilde{I}_1^{R1,F} & \tilde{I}_2^{R1,F} & \tilde{I}_0^{R1,F} \end{bmatrix}^T \quad (25)$$

Combining equation (22) and (24), the new equation including x can be rearranged as (26),

$$\begin{aligned} &\gamma_1 \cosh(-\gamma_1 xl)\tilde{V}_1^{S1,F} + Z_1 \sinh(-\gamma_1 xl)\tilde{I}_1^{S1,F} \\ &= \gamma_1 \cosh[-\gamma_1 l - (-\gamma_1 xl)]\tilde{V}_1^{R1,F} + Z_1 \sinh[-\gamma_1 l - (-\gamma_1 xl)]\tilde{I}_1^{R1,F} \end{aligned} \quad (26)$$

Then the noniterative solution of fault location can be found as (27),

$$x = \left[arctanh^{-1}\left[\frac{\gamma_1 \tilde{V}_1^{R1,F}\cosh(-\gamma_1 l) + Z_1 \tilde{I}_1^{R1,F}\sinh(-\gamma_1 l) - \gamma_1 \tilde{V}_1^{S1,F}}{Z_1 \tilde{I}_1^{S1,F} + \gamma_1 \tilde{V}_1^{R1,F}\sinh(-\gamma_1 l) + Z_1 \tilde{I}_1^{R1,F}\cosh(-\gamma_1 l)}\right] \right] \Big/ (-\gamma_1 l) \quad (27)$$

In (27), the variables $\tilde{V}_1^{R1,F}$, $\tilde{I}_1^{R1,F}$, $\tilde{V}_1^{S1,F}$ and $\tilde{I}_1^{S1,F}$ are calculated by (23) and (25). And γ_1 and Z_1 can be solved by (12) and (14). Therefore, the fault location $\times$ can be directly calculated utilizing (27) with the closed-form solution.

(b) when the fault occurs on the section 2 line

Fig. 2 shows the practically transposed lines when the fault occurs on Section 2. Similarly, the physical laws can be expressed as (28) and (29),

$$M^{-1}e^{-xlB}MK_1M^{-1}e^{-lB}M\begin{bmatrix} \tilde{V}_{abc}^{S,F} & \tilde{I}_{abc}^{S,F} \end{bmatrix}^T = \begin{bmatrix} \tilde{V}_{abc}^{f,F} & \tilde{I}_{abc}^{f1,F} \end{bmatrix}^T \quad (28)$$

$$M^{-1}e^{-(1-x)lB}MK_2M^{-1}e^{-lB}MK_2\begin{bmatrix} \tilde{V}_{abc}^{R,F} & \tilde{I}_{abc}^{R,F} \end{bmatrix}^T e^{j\delta} = \begin{bmatrix} \tilde{V}_{abc}^{f,F} & \tilde{I}_{abc}^{f2,F} \end{bmatrix} \quad (29)$$

Comparing the equation (28) and (7), both of the parts $\begin{bmatrix} \tilde{V}_{abc}^{S,F} & \tilde{I}_{abc}^{S,F} \end{bmatrix}^T$ in (7) and $K_1M^{-1}e^{-lB}M\begin{bmatrix} \tilde{V}_{abc}^{S,F} & \tilde{I}_{abc}^{S,F} \end{bmatrix}^T$ in (28) can be calculated directly as the known variables according the three phase voltage and current phasors at both terminals and the line parameters $\boldsymbol{Z}_{abc}$ and $\boldsymbol{Y}_{abc}$. Meanwhile, the remaining parts $M^{-1}e^{-xlB}M$ and $\begin{bmatrix} \tilde{V}_{abc}^{f,F} & \tilde{I}_{abc}^{f1,F} \end{bmatrix}^T$ are the same in (7) and (28). Define the formula (30),

$$\begin{bmatrix} \tilde{V}_{abc}^{S2,F} & \tilde{I}_{abc}^{S2,F} \end{bmatrix}^T = K_1M^{-1}e^{-lB}M\begin{bmatrix} \tilde{V}_{abc}^{S,F} & \tilde{I}_{abc}^{S,F} \end{bmatrix}^T \quad (30)$$

Substitute (30) into (28),

$$M^{-1}e^{-xlB}M\begin{bmatrix} \tilde{V}_{abc}^{S2,F} & \tilde{I}_{abc}^{S2,F} \end{bmatrix}^T = \begin{bmatrix} \tilde{V}_{abc}^{f,F} & \tilde{I}_{abc}^{f1,F} \end{bmatrix}^T \quad (31)$$

Therefore, equation (31) has a similar formulation as equation (7). Therefore, with similar procedure, after decoupling in 120 domain, the row including $\tilde{V}_1^{f,F}$ can be written as (32),

$$\tilde{V}_1^{f,F} = \cosh(-\gamma_1 xl)\tilde{V}_1^{S2,F} + Z_1 \sinh(-\gamma_1 xl)\tilde{I}_1^{S2,F}/\gamma_1 \quad (32)$$

where the parameters γ_1 and Z_1 are solved by (12) and (14), and $\tilde{V}_1^{S2,F}$, $\tilde{I}_1^{S2,F}$ are defined as (33). The superscripts "2″ denotes the scenario where the fault occurs within section 2,

$$\begin{bmatrix} T_V & 0 \\ 0 & T_I \end{bmatrix}^{-1} \begin{bmatrix} \tilde{V}_{abc}^{S2,F} & \tilde{I}_{abc}^{S2,F} \end{bmatrix}^T = \begin{bmatrix} \tilde{V}_1^{S2,F} & \tilde{V}_2^{S2,F} & \tilde{V}_0^{S2,F} & \tilde{I}_1^{S2,F} & \tilde{I}_2^{S2,F} & \tilde{I}_0^{S2,F} \end{bmatrix}^T \quad (33)$$

Similarly, the difference between equation (11) and equation (29) are the part $[N_1 \quad N_2]^T$ in (11) and the part $K_2M^{-1}e^{-lB}MK_2\begin{bmatrix} \tilde{V}_{abc}^{R,F} & \tilde{I}_{abc}^{R,F} \end{bmatrix}^T e^{j\delta}$ in (29). Define the formula (34),

$$[N_{21} \quad N_{22}]^T = K_2M^{-1}e^{-lB}MK_2\begin{bmatrix} \tilde{V}_{abc}^{R,F} & \tilde{I}_{abc}^{R,F} \end{bmatrix}^T e^{j\delta} \quad (34)$$

Substituting (34) in (29),

$$M^{-1}e^{-(1-x)lB}M[N_{21} \quad N_{22}]^T = \begin{bmatrix} \tilde{V}_{abc}^{f,F} & \tilde{I}_{abc}^{f2,F} \end{bmatrix} \quad (35)$$

Because equation (35) and equation (11) own the same formulation, equation (35) can be similarly decoupled as,

$$\tilde{V}_1^{f,F} = \cosh[-\gamma_1(1-x)l]\tilde{V}_1^{R2,F} + Z_1 \sinh[-\gamma_1(1-x)l]\tilde{I}_1^{R2,F}/\gamma_1 \quad (36)$$

where $\tilde{V}_1^{R2,F}$ and $\tilde{I}_1^{R2,F}$ can be calculated by (37), and the superscripts "2″ denotes the scenario where the fault occurs within section 2,

$$\begin{bmatrix} T_V & 0 \\ 0 & T_I \end{bmatrix}^{-1} \begin{bmatrix} N_{21} \\ N_{22} \end{bmatrix} = \begin{bmatrix} \tilde{V}_1^{R2,F} & \tilde{V}_2^{R2,F} & \tilde{V}_0^{R2,F} & \tilde{I}_1^{R2,F} & \tilde{I}_2^{R2,F} & \tilde{I}_0^{R2,F} \end{bmatrix}^T \quad (37)$$

By (32) and (36), the problem of fault location can be expressed as (38),

$$\begin{aligned} &\cosh(-\gamma_1 xl)\tilde{V}_1^{S2,F} + Z_1 \sinh(-\gamma_1 xl)\tilde{I}_1^{S2,F}/\gamma_1 \\ &= \cosh[-\gamma_1(1-x)l]\tilde{V}_1^{R2,F} + Z_1 \sinh[-\gamma_1(1-x)l]\tilde{I}_1^{R2,F}/\gamma_1 \end{aligned} \quad (38)$$

Then the closed-form solution of x can be obtained,

$$x = \left[arctanh^{-1}\left[\frac{\gamma_1 \tilde{V}_1^{R2,F}\cosh(-\gamma_1 l) + Z_1 \tilde{I}_1^{R2,F}\sinh(-\gamma_1 l) - \gamma_1 \tilde{V}_1^{S2,F}}{Z_1 \tilde{I}_1^{S2,F} + \gamma_1 \tilde{V}_1^{R2,F}\sinh(-\gamma_1 l) + Z_1 \tilde{I}_1^{R2,F}\cosh(-\gamma_1 l)}\right] \right] \Big/ (-\gamma_1 l) \quad (39)$$

(c) when the fault occurs on the section 3 line

Fig. 3 shows the practically transposed lines when the fault occurs on

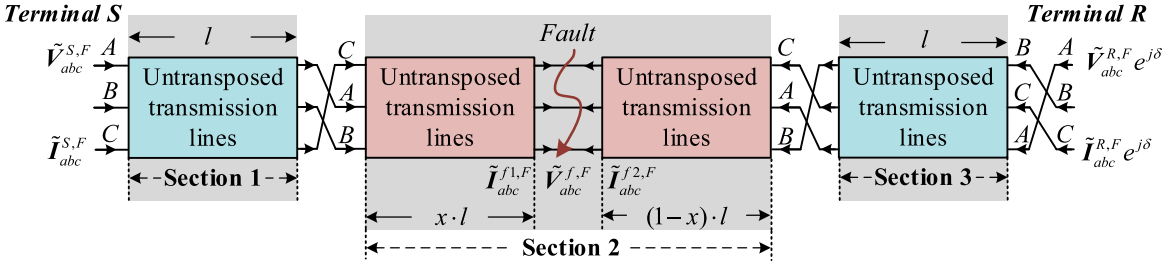

Fig. 2. The practically transposed lines when the fault occurs on Section 2.

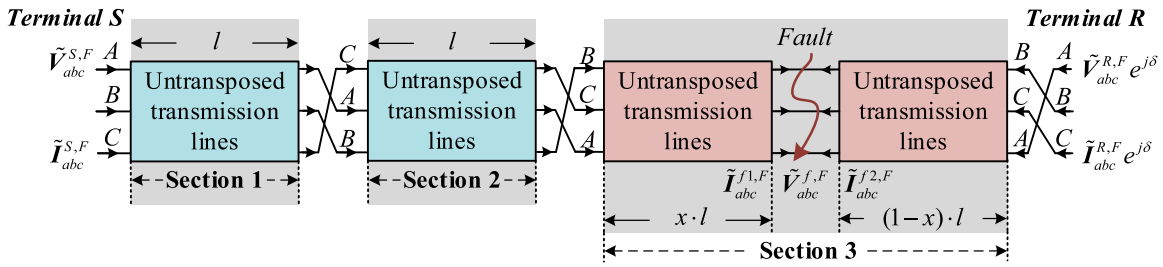

Fig. 3. The practically transposed lines when the fault occurs on Section 3.

Section 3. According to the physical laws,

$$\mathrm{M}^{-1}e^{-x\mathrm{lB}}\mathrm{M}\mathrm{K}_1\mathrm{M}^{-1}e^{-\mathrm{lB}}\mathrm{M}\mathrm{K}_1\mathrm{M}^{-1}e^{-\mathrm{lB}}\mathrm{M}\begin{bmatrix}\widetilde{\mathrm{V}}_{abc}^{S,F} & \widetilde{\mathrm{I}}_{abc}^{S,F}\end{bmatrix}^T=\begin{bmatrix}\widetilde{\mathrm{V}}_{abc}^{f,F} & \widetilde{\mathrm{I}}_{abc}^{f1,F}\end{bmatrix}^T \quad (40)$$

$$\mathrm{M}^{-1}e^{-(1-x)\mathrm{lB}}\mathrm{M}\mathrm{K}_2\begin{bmatrix}\widetilde{\mathrm{V}}_{abc}^{R,F} & \widetilde{\mathrm{I}}_{abc}^{R,F}\end{bmatrix}^T e^{j\delta}=\begin{bmatrix}\widetilde{\mathrm{V}}_{abc}^{f,F} & \widetilde{\mathrm{I}}_{abc}^{f2,F}\end{bmatrix}^T \quad (41)$$

To simplify the expressions of equation (40) and (41), define (42) and (43)

$$\begin{bmatrix}\widetilde{\mathrm{V}}_{abc}^{S3,F} & \widetilde{\mathrm{I}}_{abc}^{S3,F}\end{bmatrix}^T=\mathrm{K}_1\mathrm{M}^{-1}e^{-\mathrm{lB}}\mathrm{M}\mathrm{K}_1\mathrm{M}^{-1}e^{-\mathrm{lB}}\mathrm{M}\begin{bmatrix}\widetilde{\mathrm{V}}_{abc}^{S,F} & \widetilde{\mathrm{I}}_{abc}^{S,F}\end{bmatrix}^T \quad (42)$$

$$\begin{bmatrix}\mathrm{N}_{31} & \mathrm{N}_{32}\end{bmatrix}^T=\mathrm{K}_2\begin{bmatrix}\widetilde{\mathrm{V}}_{abc}^{R,F} & \widetilde{\mathrm{I}}_{abc}^{R,F}\end{bmatrix}^T e^{j\delta} \quad (43)$$

Substituting (42) and (43) into (40) and (41), respectively. Equations (44) and (45) can be obtained,

$$\mathrm{M}^{-1}e^{-x\mathrm{lB}}\mathrm{M}\begin{bmatrix}\widetilde{\mathrm{V}}_{abc}^{S3,F} & \widetilde{\mathrm{I}}_{abc}^{S3,F}\end{bmatrix}^T=\begin{bmatrix}\widetilde{\mathrm{V}}_{abc}^{f,F} & \widetilde{\mathrm{I}}_{abc}^{f1,F}\end{bmatrix}^T \quad (44)$$

$$\mathrm{M}^{-1}e^{-(1-x)\mathrm{lB}}\mathrm{M}\begin{bmatrix}\mathrm{N}_{31} & \mathrm{N}_{32}\end{bmatrix}^T=\begin{bmatrix}\widetilde{\mathrm{V}}_{abc}^{f,F} & \widetilde{\mathrm{I}}_{abc}^{f2,F}\end{bmatrix}^T \quad (45)$$

One can observe that (31) and (44) have the similar formulation. Therefore, (44) can be decoupled as (46),

$$\widetilde{V}_1^{f,F}=\cosh(-\gamma_1 xl)\widetilde{V}_1^{S3,F}+Z_1\sinh(-\gamma_1 xl)\widetilde{I}_1^{S3,F}/\gamma_1 \quad (46)$$

where $\widetilde{V}_1^{S3,F}$, $\widetilde{I}_1^{S3,F}$ are calculated by (47), and the superscripts "3″ denotes the scenario where the fault occurs within section 3,

$$\begin{bmatrix}\mathrm{T}_V & 0\\ 0 & \mathrm{T}_I\end{bmatrix}^{-1}\begin{bmatrix}\widetilde{\mathrm{V}}_{abc}^{S3,F} & \widetilde{\mathrm{I}}_{abc}^{S3,F}\end{bmatrix}^T=\begin{bmatrix}\widetilde{V}_1^{S3,F} & \widetilde{V}_2^{S3,F} & \widetilde{V}_0^{S3,F} & \widetilde{I}_1^{S3,F} & \widetilde{I}_2^{S3,F} & \widetilde{I}_0^{S3,F}\end{bmatrix}^T \quad (47)$$

Similar as (35), equation (43) can be also decoupled as (48),

$$\widetilde{V}_1^{f,F}=\cosh[-\gamma_1(1-x)l]\widetilde{V}_1^{R3,F}+Z_1\sinh[-\gamma_1(1-x)l]\widetilde{I}_1^{R3,F}/\gamma_1 \quad (48)$$

where $\widetilde{V}_1^{R3,F}$ and $\widetilde{I}_1^{R3,F}$ can be calculated by (49), and the superscripts "3″ denotes the scenario where the fault occurs within section 3,

$$\begin{bmatrix}\mathrm{T}_V & 0\\ 0 & \mathrm{T}_I\end{bmatrix}^{-1}\begin{bmatrix}\mathrm{N}_{31}\\ \mathrm{N}_{32}\end{bmatrix}=\begin{bmatrix}\widetilde{V}_1^{R3,F} & \widetilde{V}_2^{R3,F} & \widetilde{V}_0^{R3,F} & \widetilde{I}_1^{R3,F} & \widetilde{I}_2^{R3,F} & \widetilde{I}_0^{R3,F}\end{bmatrix}^T \quad (49)$$

Therefore, when the fault occurs on the Section 3, the fault location problem can be expressed as (50),

$$\begin{aligned}&\cosh(-\gamma_1 xl)\widetilde{V}_1^{S3,F}+Z_1\sinh(-\gamma_1 xl)\widetilde{I}_1^{S3,F}/\gamma_1\\ &=\cosh[-\gamma_1(1-x)l]\widetilde{V}_1^{R3,F}+Z_1\sinh[-\gamma_1(1-x)l]\widetilde{I}_1^{R3,F}/\gamma_1\end{aligned} \quad (50)$$

The closed-form solution of x can be obtained as,

$$x=\left[arctanh^{-1}\left[\frac{\gamma_1\widetilde{V}_1^{R3,F}\cosh(-\gamma_1 l)+Z_1\widetilde{I}_1^{R3,F}\sinh(-\gamma_1 l)-\gamma_1\widetilde{V}_1^{S3,F}}{Z_1\widetilde{I}_1^{S3,F}+\gamma_1\widetilde{V}_1^{R3,F}\sinh(-\gamma_1 l)+Z_1\widetilde{I}_1^{R3,F}\cosh(-\gamma_1 l)}\right]\right]\Big/(-\gamma_1 l) \quad (51)$$

(d) Faulted line section identification

In part 3.2(a)-(c) of the paper, the expressions of fault location during three possible fault scenarios are derived in detail. However, when a fault occurs in a practically transposed line, it is important to determine the faulted line section, and to decide which expression corresponds to the correct fault location.

In this paper, the faulted line section procedure is rather simple. With available voltage and current phasor measurements, we can assume that the fault occurs at any one of the untransposed line section, and use the corresponding expression to calculate the fault location. This will result in three calculated fault location x. From the fact that $0 < x < 1$, one can neglect two unreasonable roots and determine the correct roots.

To sum up, the proposed fault location method constructs the model of practically transposed transmission lines utilizing three untransposed line sections according to the principle of transposition. The proposed method fully considers the distributed parameters as well as asymmetry of the practically transposed lines during the fault. At the same time, the proposed method provides the closed-form noniterative solution of fault location, without requiring the synchronized measurements at terminals.

4. Numerical experiments

In order to test the performance of the proposed fault location method, a 500 kV two-terminal three phase practically transposed transmission line system is built in PSCAD/EMTDC as Fig. 4. The 150 km practically transposed lines are constructed by three untransposed line sections (each untransposed line is 50 km and the frequency dependent (phase) transmission line model is selected in PSCAD/EMTDC). The nominal frequency of the system is 50 Hz. Three phase voltage and current measurements are installed at both terminals of the transmission line. In the testing system, three phase instantaneous voltages and currents are firstly captured and stored in COMTRADE files with 4000 sampling rate according to IEC61850-9-2LE standard [26]. As the proposed fault location method is based on phasor domain, the accuracy of phasor estimation may influence the results of fault location. Some existing phasor estimation methods have been proposed in [27–28] to improve the accuracy of phasor estimation during severe transients as well. Since the scope of the paper is not phasor extraction during severe transients, the data window for phasor calculation is selected as 3rd cycle to 4th cycle after the fault, and the three phase voltage and current phasors at both terminals before and during the fault are calculated by IEEE C37. 118 standard [29]. The unsynchronized angle of 30° is added to the three phase voltage and current phasors at the terminal R to verify the performance of the proposed method with the influence of the unsynchronized measurements.

In the test system, the parameters are set as follows. The three phase power source at terminal S is with the source impedance of $10\angle 80^\circ\ \Omega$, and the phase angle of 30°. The three phase power source at terminal R is with the source impedance of $15\angle 75^\circ\ \Omega$, and the phase angle of 0°. For the untransposed lines, the series impedance matrix and the shunt

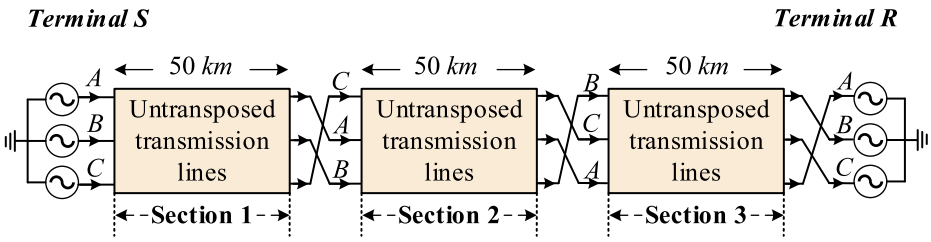

Fig. 4. An example test system in PSCAD.

admittance matrix are shown as below.

$$Z_{abc} = \begin{bmatrix} 0.0900 + j0.4714 & 0.0880 + j0.2579 & 0.0840 + j0.2179 \\ 0.0880 + j0.2579 & 0.0979 + j0.4669 & 0.0880 + j0.2579 \\ 0.0840 + j0.2179 & 0.0880 + j0.2579 & 0.0900 + j0.4714 \end{bmatrix} \times 10^{-3} \ (\boldsymbol{ohms/m})$$

$$Y_{abc} = \begin{bmatrix} 0.001 + j0.4195 & -j0.1013 & -j0.0304 \\ -j0.1013 & 0.001 + j0.4562 & -j0.1013 \\ -j0.0304 & -j0.1013 & 0.001 + j0.4195 \end{bmatrix} \times 10^{-8} \ (\boldsymbol{mhos/m})$$

In addition, the existing method [23] is selected in comparison to the proposed method. It assumes ideal transposition of transmission line, and fully considers the distributed parameter of the line without requiring the synchronized measurements at both terminals. Through this comparison, the importance to consider practical transposition of transmission line can be clearly demonstrated. The accuracy of the fault location methods is expressed by the absolute errors (in percentage), which is shown in (52),

$$Error(\%) = \left| \frac{Estimated\ Fault\ Location - Actual\ Fault\ Location}{Line\ Length} \right| \times 100\% \tag{52}$$

It is worth noting that the results of the identification of faulted untransposed line section strictly follows the description in part 3.2(d). Here the testing cases of phase A to ground faults with 0.01 O fault impedance at different fault locations in section 2 line (0.10, 0.50 and 0.98p.u.) are selected as examples. The fault location results are shown in Table 1. One can clearly observe that the estimated location $\times$ satisfies $0 < x < 1$ only when the fault is assumed to occur within section 2 line. Therefore, the proposed logic of faulted line section identification is reliable.

Next, extensive fault testing cases are studied with different fault types, fault locations and fault impedances in the following parts.

4.1. Single phase to ground faults

This part studies 124 phase *A* to ground fault cases with 31 different fault locations *L* (every 5 km through the line including 1 km and 149 km) and 4 different fault impedances R_f (0.01 Ω, 1 O, 5 Ω and 10 Ω). The absolute fault location errors (in percentage) of the proposed method and the existing method are shown in Fig. 5 and Table 2. One can observe that the proposed method presents higher accuracy compared to the existing method for different fault location and fault impedance cases. The maximum absolute fault location errors of the proposed method and the existing method are 0.0999% and 1.5624%, respectively. From the results, one can observe that the accuracy of the proposed fault location method is higher than that of the existing method, as the proposed method accurately considers the asymmetry of practically transposed transmission lines during the fault. On the contrary, the existing method neglects the line asymmetry during the fault.

Also, one can observe an "M" shaped fault location error for the existing method. The reason is explained as follows. When the fault occurred close to either terminal of the practically transposed line, the fault separates the entire line as two parts: one part is with very small length, while the other part is the entire practically transposed line. In this case, the practically transposed line can be treated approximated as an ideally transposed line. Therefore the fault location error of the existing method is small at line terminals. When the fault occurs close to the midpoint of the practically transposed line, the transposition will also reduce the asymmetry of the overall transmission line [20]. In this case, the fault location error of the existing method will also be small.

Table 1
The results of faulted line section identification.

Actual location of the fault in section 2 line (p.u.)	Estimated location from section 1 formulation (p.u.)	Estimated location from section 2 formulation (p.u.)	Estimated location from section 3 formulation (p.u.)
0.10	1.1041	0.1002	−0.9347
0.50	1.5194	0.5000	−0.5195
0.98	2.0180	0.9800	−0.0208

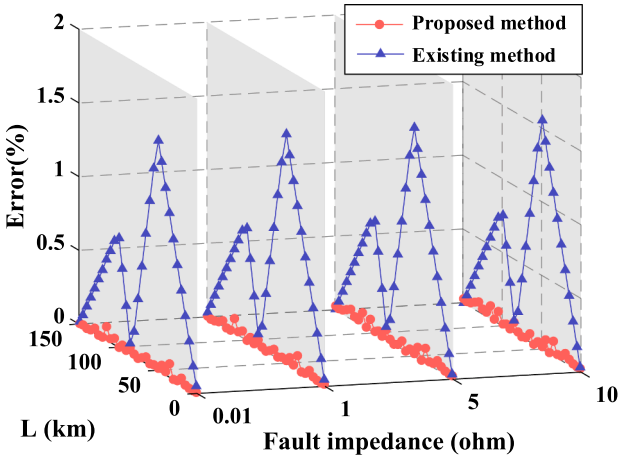

Fig. 5. Results comparison, low impedance A-G faults, different fault locations and impedances.

Table 2
Comparison of average and maximum errors, low impedance A-G faults, different fault locations and impedances.

Fault impedance (Ω)	Proposed method		Existing method	
	Avg abs error (%)	Max abs error (%)	Avg abs error (%)	Max abs error (%)
0.01	0.0222	0.0923	0.5975	1.5624
1	0.0242	0.0988	0.6056	1.5576
5	0.0353	0.0999	0.5972	1.5533
10	0.0366	0.0995	0.5944	1.5548

4.2. Phase to phase faults

This part studies 124 phase *B* to phase *C* fault cases with 31 different fault locations *L* (every 5 km through the line including 1 km and 149 km) and 4 different fault impedances R_f (0.01 Ω, 1 Ω, 5 Ω and 10 Ω). The absolute fault location errors (in percentage) of the proposed method and the existing method are shown in Fig. 6 and Table 3. The maximum absolute fault location errors of the proposed method and the existing method are 0.0172% and 2.0981%, respectively. The proposed method still demonstrates less fault location errors than the existing method.

4.3. Phase to phase to ground faults

This part studies 124 phase *B* to phase *C* to ground fault cases with 31 different fault locations *L* (every 5 km through the line including 1 km and 149 km) and 4 different fault impedances R_f (0.01 Ω, 1 Ω, 5 Ω and 10 Ω). The absolute fault location errors (in percentage) of the proposed method and the existing method are shown in Fig. 7 and Table 4. The maximum absolute fault location errors of the proposed method and the existing method are 0.1003% and 1.4234%, respectively. The proposed method also demonstrates less fault location errors than the existing method.

4.4. Three phase faults

This part studies 124 three phase fault cases with 31 different fault locations *L* (every 5 km through the line including 1 km and 149 km) and 4 different fault impedances R_f (0.01 Ω, 1 Ω, 5 Ω and 10 Ω). The absolute fault location errors (in percentage) of the proposed method and the existing method are shown in Fig. 8 and Table 5. Moreover, the maximum absolute fault location errors of the proposed method and the existing method are 0.0649% and 0.1123%, respectively. One can observe that the fault location accuracy of the existing method is not much influenced with the assumption of the practically transposed lines during the three phase symmetrical fault. The proposed method has slightly improved accuracy than the existing method.

4.5. High impedance faults

To validate the performance of the proposed method in high fault impedances, this part studies 124 phase *A* to ground fault cases with 31 different fault locations *L* (every 5 km through the line including 1 km and 149 km) and 4 different fault impedances R_f (100 Ω, 200 Ω, 300 Ω and 500 Ω). The absolute fault location errors (in percentage) of the proposed method and the existing method are shown in Fig. 9 and

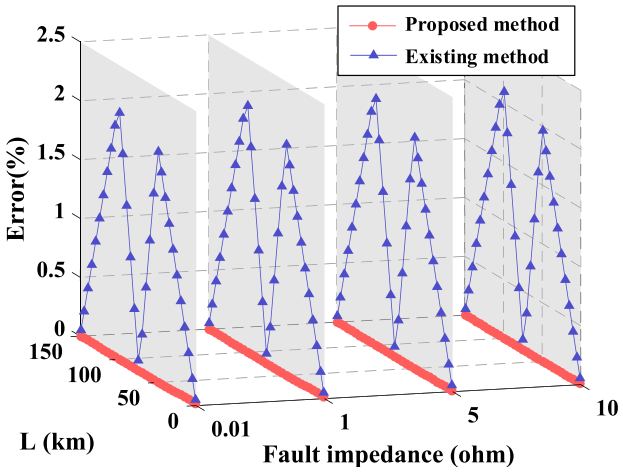

Fig. 6. Results comparison, low impedance B-C faults, different fault locations and impedances.

Table 3
Comparison of average and maximum errors, low impedance B-C faults, different fault locations and impedances.

Fault impedance (Ω)	Proposed method		Existing method	
	Avg abs error (%)	Max abs error (%)	Avg abs error (%)	Max abs error (%)
0.01	0.0054	0.0172	1.0186	2.0981
1	0.0054	0.0152	1.0186	2.0971
5	0.0034	0.0073	1.0193	2.0972
10	0.0034	0.0070	1.0195	2.0974

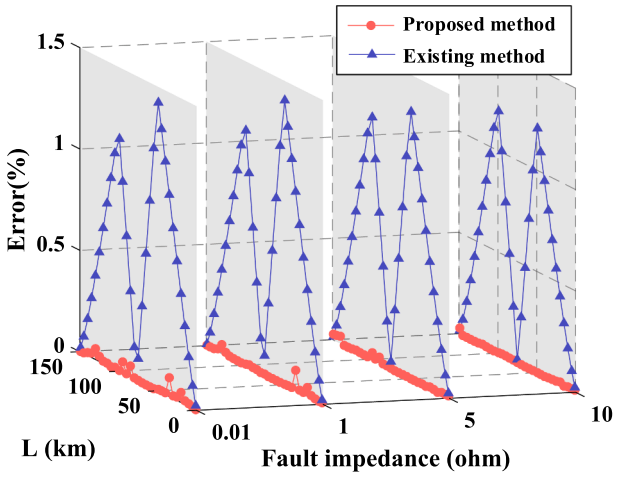

Fig. 7. Results comparison, low impedance B-C-G faults, different fault locations and impedances.

Table 4
Comparison of average and maximum errors, low impedance B-C-G faults, different fault locations and impedances.

Fault impedance (Ω)	Proposed method		Existing method	
	Avg abs error (%)	Max abs error (%)	Avg abs error (%)	Max abs error (%)
0.01	0.0171	0.0933	0.6225	1.4234
1	0.0117	0.1003	0.6180	1.4048
5	0.0083	0.0362	0.6024	1.3186
10	0.0043	0.0298	0.5725	1.2075

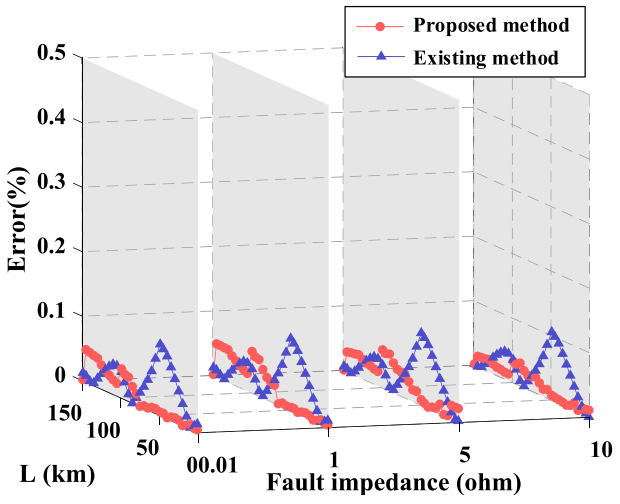

Fig. 8. Results comparison, low impedance three phase faults, different fault locations and impedances.

Table 5
Comparison of average and maximum errors, low impedance three phase faults, different fault locations and impedances.

Fault impedance (Ω)	Proposed method		Existing method	
	Avg abs error (%)	Max abs error (%)	Avg abs error (%)	Max abs error (%)
0.01	0.0186	0.0508	0.0377	0.1108
1	0.0246	0.0649	0.0373	0.1118
5	0.0249	0.0594	0.0377	0.1123
10	0.0146	0.0356	0.0361	0.1058

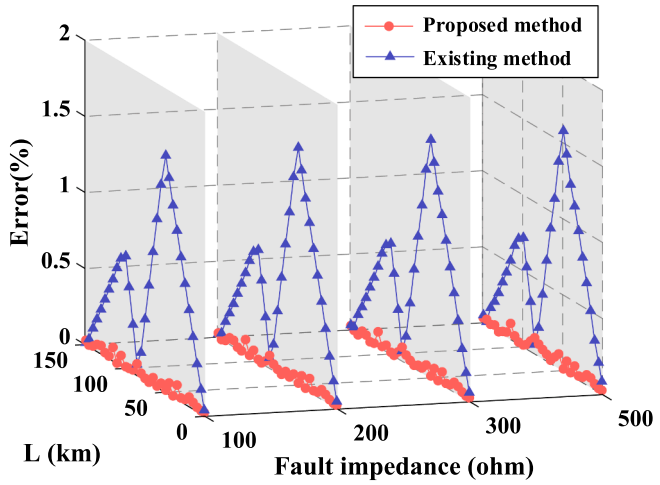

Fig. 9. Results comparison, high impedance A-G faults, different fault locations and impedances.

Table 6
Comparison of average and maximum errors, high impedance A-G faults, different fault locations and impedances.

Fault impedance (Ω)	Proposed method		Existing method	
	Avg abs error (%)	Max abs error (%)	Avg abs error (%)	Max abs error (%)
100	0.0355	0.0955	0.5929	1.5604
200	0.0353	0.0953	0.5935	1.5551
300	0.0373	0.0989	0.5946	1.5699
500	0.0455	0.1062	0.5979	1.5800

Table 6. The maximum absolute fault location errors of the proposed method and the existing method are 0.1003% and 1.4234%, respectively. The proposed method also shows improved accuracy compared to the existing method.

5. Discussion

To further validate the performance of the proposed fault location method, additional testing cases are studied in the example system in Fig. 4. The following test cases study the impact of different unsynchronized angles, loading conditions, measurement noises and line length on the fault location accuracy.

5.1. Estimation of different unsynchronized angles

This part provides the testing cases with different unsynchronized angles for the proposed method. The unsynchronized angles are selected −180°, −90°, −45°, 70°, 130° and 180°, respectively. The values and the absolute deviations of the estimated angles are shown in Table 7. One can observe that the maximum deviation is only 0.0002°. One can conclude that the performance of the proposed method is not affected by the unsynchronized angle.

5.2. Effect of different loading conditions

This part provides the testing cases with different loading conditions for the proposed method. The 93 fault events are phase *A* to ground faults with 100 Ω fault impedance, with 31 different fault locations *L* (every 5 km through the line including 1 km and 149 km) and 3 different loading conditions. The different loading conditions are represented by the different phase angles of power sources at both terminals. The absolute fault location errors (in percentage) of the proposed method and the existing method are shown in Fig. 10 and Table 8. The proposed fault location method is not affected by various loading conditions.

5.3. Effect of different measurement noises

This part provides the testing cases with different measurement noises for the proposed method. The 93 fault cases are phase A to ground faults with 100 Ω fault impedance, with 31 different fault locations *L* (every 5 km through the line including 1 km and 149 km) and 3 different measurement noises, which are added to the instantaneous measurements in COMTRADE file according to the Gaussian noises. The absolute fault location errors (in percentage) of the proposed method and the existing method are shown in Fig. 11 and Table 9. Although the accuracy of the proposed method is influenced by the measurement noises slightly, one can observe that the proposed method presents higher accuracy compared to the existing methods, independent of fault locations and measurement noises.

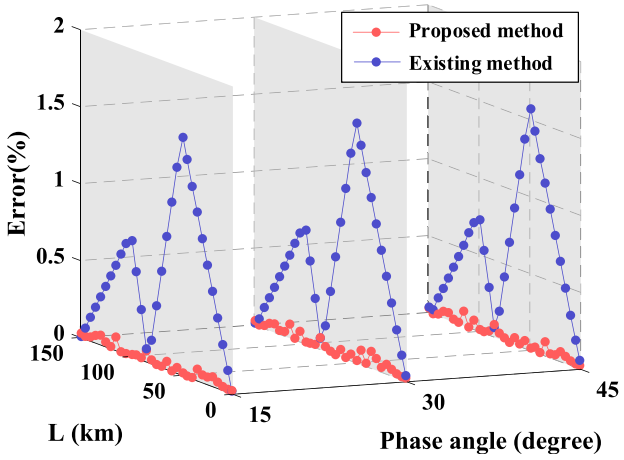

Fig. 10. Results comparison, 100 Ω A-G faults, different fault locations and phase angles.

Table 7
The estimation of unsynchronized angles for the proposed method.

The real angle (degree)	−180	−90	−45	70	130	180
The estimated angle (degree)	−179.9998	−89.9998	−44.9998	70.0002	130.0002	180.0002
The deviation angle (degree)	0.0002	0.0002	0.0002	0.0002	0.0002	0.0002

Table 8
Comparison of average and maximum errors, 100 Ω A-G faults, different fault locations and phase angles.

Phase angle (degree)	Proposed method		Existing method	
	Avg abs error (%)	Max abs error (%)	Avg abs error (%)	Max abs error (%)
15	0.0322	0.0891	0.5917	1.5488
30	0.0393	0.1116	0.5929	1.5604
45	0.0337	0.0947	0.5941	1.5722

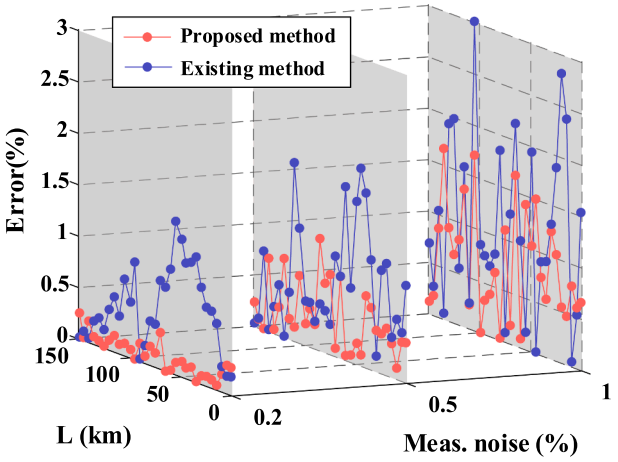

Fig. 11. Results comparison, 100 Ω A-G faults, different fault locations and Meas. Noises.

Table 9
Comparison of average and maximum errors, 100 Ω A-G faults, different fault locations and Meas. noises.

Meas. noise (%)	Proposed method		Existing method	
	Avg abs error (%)	Max abs error (%)	Avg abs error (%)	Max abs error (%)
0.2	0.1218	0.3589	0.5882	1.4968
0.5	0.3767	1.0950	0.7261	1.9272
1	0.7629	1.7107	1.1442	3.0123

5.4. Effect of different line length

This part provides the testing cases with different line length for the proposed method. The total line length is set as 450 km, which contains three untransposed transmission sections (every section is 150 km). The 64 fault cases are phase A to ground faults with different fault locations L (every 30 km through the line including 1 km and 449 km) and different fault impedances (0.01 Ω, 1 Ω, 5 Ω and 10 Ω). The absolute fault location errors (in percentage) of the proposed method and the existing method are shown in Fig. 12 and Table 10. One can observe that the proposed method still presents higher accuracy compared to the existing method. The accuracy of the proposed method is not quite affected by the length of the transmission line.

5.5. Other discussions

Although the proposed method provides the closed-form solution of fault location on practically transposed lines without requiring the synchronization, there are additional challenges to be considered. On one hand, the proposed method builds the practically transposed line model with a typical transposition strategy, which transposes the phase conductors every one-third of the total line length. However, there could be other transposition strategies with different times of transposition at different locations of the line. In those cases, the model of the practically transposed line should be adjusted to ensure accuracy. On the other hand, the proposed method typically requires accurate line parameters to calculate the fault location. However, the line parameters may be not accurate in the utility database, or could even fluctuate due to the weather and loading conditions of the line. These problems would be studied in the future.

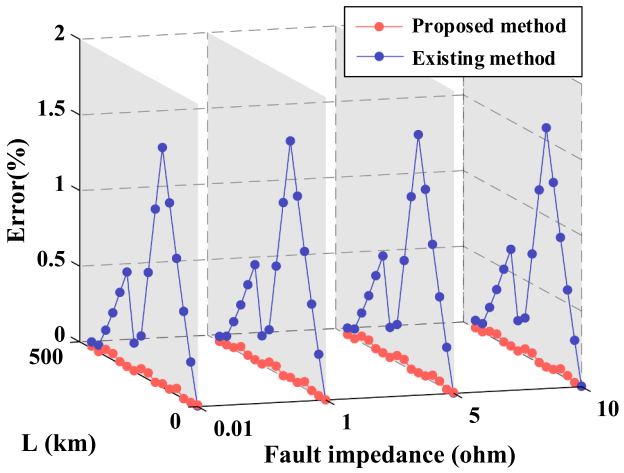

Fig. 12. Results comparison, low impedance A-G faults, different fault locations and impedances.

Table 10
Comparison of average and maximum errors, low impedance A-G faults, different fault locations and impedances.

Fault impedance (Ω)	Proposed method		Existing method	
	Avg abs error (%)	Max abs error (%)	Avg abs error (%)	Max abs error (%)
0.01	0.0202	0.0447	0.5356	1.5842
1	0.0175	0.0446	0.5386	1.5838
5	0.0198	0.0444	0.5433	1.5817
10	0.0175	0.0442	0.5430	1.5829

6. Conclusion

This paper proposes an accurate fault location method on practically transposed transmission lines with closed-form solutions. Existing fault location methods usually assume that the transmission lines are ideally transposed, which will bring modeling errors especially during line faults. In comparison, the proposed fault location method fully considers the asymmetry of practically transposed transmission lines during the fault. The proposed method also accurately models the fully distributed line parameters, and is compatible with unsynchronized measurements at terminals. Through careful deviations, the proposed method presented closed-form noniterative solutions for fault location. Simulation study validates that the proposed method owns higher accuracy of fault location than the existing method for different fault locations, fault impedances and fault types. Even with different unsynchronized angles, different loading conditions, different measurement noises and different line lengths, the proposed method still presents high fault location accuracy.

Declaration of Competing Interest

The authors declare that they have no known competing financial interests or personal relationships that could have appeared to influence the work reported in this paper.

Data availability

The authors do not have permission to share data.

Acknowledgments

This work is sponsored by National Nature Science Foundation of China (No. 51807119) and Key Laboratory of Control of Power Transmission and Conversion (SJTU), Ministry of Education (No. 2022AB01). Their support is greatly appreciated.

References

[1] Lu D, Liu Y, Xie J, Wang B, Liao Q. Multi-Layer Model Enabled Fault Location for Underground Cables in MMC-HVDC Grids Considering Distributed and Frequency Dependent Line Parameters. IEEE Trans Power Del 2022;37(4):3082–96.
[2] Alqudah M, Pavlovski M, Dokic T, Kezunovic M, Hu Y, Obradovic Z. Fault Detection Utilizing Convolution Neural Network on Timeseries Synchrophasor Data From Phasor Measurement Units. IEEE Trans Power Syst 2022;37(5):3434–42.
[3] Chang P, Song G, Hou J, Xu R. A Single-Terminal Fault Location Method for Transmission Lines Integrated by Inverter-Type Source. IEEE Trans Power Del 2022;37(3):1704–13.
[4] Wang D, Hou M, Guo Y. Travelling Wave Fault Location of HVAC Transmission Line Based on Frequency-Dependent Characteristic. IEEE Trans Power Del 2021;36(6):3496–505.
[5] Liu Y, et al. Dynamic State Estimation for Power System Control and Protection. IEEE Trans Power Systems Nov. 2021;36(6):5909–21.
[6] Naidu O, Pradhan AK. A Traveling Wave-Based Fault Location Method Using Unsynchronized Current Measurements. IEEE Trans Power Del 2019;34(2):505–13.
[7] Leite EJS, Lopes FV, Costa FB, Neves WLA. Closed-Form Solution for Traveling Wave-Based Fault Location on Non-Homogeneous Lines. IEEE Trans Power Del 2019;34(3):1138–50.
[8] Xing Y, Liu Y, Nie Y, Li R, He X. Data-Driven Transmission Line Fault Location with Single-Ended Measurements and Knowledge-Aware Graph Neural Network. IEEE Power Energy Soc Gen Meet 2022.
[9] Majidi M, Etezadi-Amoli M, Fadali MS. A Sparse-Data-Driven Approach for Fault Location in Transmission Networks. IEEE Trans Smart Grid 2017;8(2):548–56.
[10] Wang B, Liu Y, Lu D, Yue K, Fan R. Transmission Line Fault Location in MMC-HVDC Grids Based on Dynamic State Estimation and Gradient Descent. IEEE Trans Power Del 2021;36(3):1714–25.
[11] Lu D, Liu Y, Chen S, Wang B, Lu D. An Improved Noniterative Parameter-Free Fault Location Method on Untransposed Transmission Lines Using Multi-Section Models. IEEE Trans Power Del 2022;37(3):1356–69.
[12] Kalita K, Anand S, Parida SK. A Closed Form Solution for Line Parameter-Less Fault Location With Unsynchronized Measurements. IEEE Trans Power Del 2022;37(3):1997–2006.
[13] Lopes FV, Eduardo JS, Jr L, João PG, Ribeiro AB, Piardi AV, et al. Single-ended multi-method phasor-based approach for optimized fault location on transmission lines. Electr Pow Syst Res 2022;212.
[14] Stanojević VA, Preston G, Terzija V. Synchronised Measurements Based Algorithm for Long Transmission Line Fault Analysis. IEEE Trans Smart Grid 2018;9(5):4448–57.
[15] Lee Y-J, Lin T-C, Liu C-W. Multi-Terminal Nonhomogeneous Transmission Line Fault Location Utilizing Synchronized Data. IEEE Trans Power Del 2019;34(3):1030–8.
[16] Terzija V, Radojević ZM, Preston G. Flexible Synchronized Measurement Technology-Based Fault Locator. IEEE Trans Smart Grid 2015;6(2):866–73.
[17] Brahma SM, Girgis AA. Fault location on a transmission line using synchronized Voltage measurements. IEEE Trans Power Del 2004;19(4):1619–22.
[18] Vieira DAG, Oliveira DB, Lisboa AC. A Closed-Form Solution for Transmission-Line Fault Location Without the Need of Terminal Synchronization or Line Parameters. IEEE Trans Power Del 2013;28(2):1238–9.
[19] Silveira EG, Pereira C. Transmission Line Fault Location Using Two-Terminal Data Without Time Synchronization. IEEE Trans Power Syst 2007;22(1):498–9.
[20] Das S, Santoso S, Gaikwad A, Patel M. Impedance-based fault location in transmission networks: theory and application. IEEE Access 2014;2:537–57.
[21] IEEE Guide for Determining Fault Location on AC Transmission and Distribution Lines, IEEE Std C37. 114-2014.
[22] Izykowski J, Molag R, Rosolowski E, Saha MM. Accurate Location of Faults on Power Transmission Lines with Use of Two-End Unsynchronized Measurements. IEEE Trans Power Del 2006;21(2):627–33.
[23] Izykowski J, Rosolowski E, Balcerek P, Fulczyk M, Saha MM. Accurate Noniterative Fault-Location Algorithm Utilizing Two-End Unsynchronized Measurements. IEEE Trans Power Del 2011;26(2):547–55.
[24] Pereira CEM, Zanetta LC. Optimization Algorithm for Fault Location in Transmission Lines Considering Current Transformers Saturation. IEEE Trans Power Del 2005;20(2):603–8.
[25] Liu Y, Wang B, Zheng X, Lu D, Fu M, Tai N. Fault Location Algorithm for Non-Homogeneous Transmission Lines Considering Line Asymmetry. IEEE Trans Power Del 2020;35(5):2425–37.
[26] IEC Std 61850. Communication Networks and Systems in Substations; 2003.
[27] Lu D, Liu Y, Wang B, Xing Y. Generalized Phasor Estimation Method Based on DFT with DC Offset Mitigation. IEEE Power Energy Soc Gen Meet 2021.
[28] Xu S, Liu H, Bi T. A General Design Method for Phasor Estimation in Different Applications. IEEE Trans Smart Grid 2021;12(3):2307–19.
[29] IEEE Std C37. 118. 2-2011. IEEE Standard for Synchrophasor Data Transfer for Power Systems; 2011.